Am J Cancer Res 2024;14(7):3404-3418
www.ajcr.us /ISSN:2156-6976/ajcr0155375

Original Article

ASB1 inhibits prostate cancer progression by destabilizing CHCHD3 via K48-linked ubiquitination

Chunchun Zhao[1*], Zhen Xu[2*], Hongliang Que[1], Ke Zhang[1], Fei Wang[1], Ruoyun Tan[3], Caibin Fan[1]

[1]Department of Urology, The Affiliated Suzhou Hospital of Nanjing Medical University, Suzhou 215002, Jiangsu, China; [2]Department of Urology, The Affiliated Taizhou People's Hospital of Nanjing Medical University, Taizhou 225300, Jiangsu, China; [3]Department of Urology, The First Affiliated Hospital of Nanjing Medical University, Nanjing 210029, Jiangsu, China. [*]Equal contributors.

Received January 10, 2024; Accepted June 17, 2024; Epub July 15, 2024; Published July 30, 2024

Abstract: Prostate cancer is a major contributor to male mortality worldwide. In this study, we revealed that Ankyrin Repeat and SOCS Box Containing 1 (ASB1) expression was significantly decreased in prostate cancer tissues, correlating strongly with poor patient prognosis. Notably, the group with low ASB1 expression exhibited an increased proportion of M2 macrophages and showed resistance to immune checkpoint inhibitors and cisplatin, but remained sensitive to androgen-receptor-targeting drug bicalutamide. Silencing ASB1 enhanced prostate cancer cell proliferation, clonogenicity, and migration, whereas its overexpression exerted the opposite effects. Through quantitative mass spectrometry interactome analysis, we identified 37 novel proteins interacting with ASB1, including CHCHD3. Subsequent experiments including co-immunoprecipitation, cycloheximide treatment, and ubiquitination assays, revealed that ASB1 interacts with CHCHD3, promoting its degradation via K48-linked ubiquitination. Cell rescue experiments further demonstrated that ASB1 inhibits prostate cancer cell through the CHCHD3/reactive oxygen species (ROS) pathway. Taken together, our study indicated that ASB1 functions as a tumor suppressor by inhibiting CHCHD3/ROS signaling, thereby playing a vital part in prevention of prostate cancer proliferation, clonogenicity, and migration.

Keywords: ASB1, CHCHD3, ubiquitination, prostate cancer

Introduction

Prostate cancer ranks as one of the most prevalent malignancies affecting males and remains the second leading cause of cancer-related deaths worldwide [1]. Treatment options are tailored to the specific characteristics of each tumor, including its type, grade, stage, and potential for recurrence. For instance, low-risk or localized prostate cancer typically involves a combination of radical prostatectomy and radiation therapy, while aggressive and metastatic cancers may require a variety of targeted therapies such as hormone therapy, chemotherapy, and immunotherapy [2]. Despite remarkable advances in optimizing these treatment strategies and improving patient quality of life, prostate cancer mortality rates have shown an upward trend in recent years [3]. Moreover, patients tend to develop resistance to standard treatment regimens over time. These challenges have spurred ongoing research to identify novel molecules and signaling pathways that contribute to prostate cancer growth, metastasis, and progression, with the goal of preventing prostate cancer metastasis and enhancing patient outcomes.

Ubiquitination, a crucial post-translational modification process, involves the attachment of a 76-amino-acid ubiquitin protein to a target protein, influencing its localization and stability [4]. In this process, E3 ubiquitin ligases play a pivotal role in the ultimate step, in which they are responsible for recognizing the target protein and facilitating ubiquitin transfer by E2 enzymes [5]. In addition, E3 ubiquitin ligases are implicated in various aspects of prostate cancer, including tumorigenesis, proliferation, response to androgen deprivation therapy, and the development of drug resistance [6-8]. The ASB family of proteins comprises a group of E3

ubiquitin ligases characterized by an N-terminal ankyrin protein repeat structural domain [9], which facilitates substrate recognition, and a C-terminal suppressor of cytokine signaling (SOCS) box that aids in protein ubiquitylation [10]. Most ASB proteins mediate ubiquitination by recruiting target proteins through ankyrin protein repeat sequences within the SOCS box structural domain. ASB1, a key member of the ASB family, is significantly associated with development and fertility in mice [11]. Additionally, its aberrant methylation is linked to left ventricular manifestations of ischemic cardiomyopathy. Epigenetic alterations of the ASB1 gene have also been implicated in anxiety-related immune dysregulation and are strongly correlated with nasopharyngeal carcinoma metastasis [12-14]. Nevertheless, the role of ASB1 on prostate cancer progression and the underlying mechanisms of its influence require further exploration.

In this study, we performed a comprehensive analysis of ASB1 expression and its prognostic significance in prostate cancer by analyzing data from The Cancer Genome Atlas (TCGA) and Genotypic Tissue Expression project (GTEx). We manipulated ASB1 levels through knockdown and overexpression techniques in two prostate cancer cell lines, both *in vitro* and *in vivo*, to explore its potential role. Our investigation extended to co-immunoprecipitation (Co-IP) assays and mass spectrometry (MS) analysis to further identify candidate binding proteins associated with ASB1, as well as cycloheximide (CHX) assays, ubiquitination assays, and cell rescue assays to demonstrate that ASB1 exerts inhibitory effects on prostate cancer progression. This inhibition is mediated through CHCHD3, a novel target molecule that is crucial in maintaining mitochondrial structure and function and influences cellular proliferation via oxidative stress pathways.

Material and methods

Bioinformatics analysis

We analyzed the expression levels of ASB1 and CHCHD3 and their correlations with the prognosis of prostate cancer patients by analyzing data from TCGA and GTEx. Patients were categorized into high and low expression groups based on the median expression level of ASB1. The degree of immune cell infiltration in these groups was assessed using the CIBERSORT algorithm. We also examined the function of checkpoint inhibitors, which operate through immune checkpoint molecules on immune cells contributing to tumor immune evasion by analyzing immune checkpoint molecules expression in both groups. Drug sensitivity for each group was evaluated based on half-maximal inhibitory concentration (IC50) values using pRRophetic algorithm.

Cell culture and transfection

Two human prostate cancer cell lines, PC3 and DU145, were obtained from Zhong Qiao Xin Zhou Biotechnology Company (Shanghai, China) and cultured in RPMI-1640 medium supplemented with 10% fetal bovine serum (Gibco, CA, USA). The cell lines were cultured at 37°C in a humidified incubator containing 5% CO_2. For transient knockdown, cells were transfected with siRNAs targeting ASB1 (si-ASB1) and CHCHD3 (si-CHCHD3) using Lipofectamine 2000 (Invitrogen, USA) [15, 16]. The siRNA sequences were listed as follows: si-ASB1-1, 5'-CUGGGUACUCUCUAGGUGC-3'; si-ASB1-2, 5'-UUCCCACUUCACUAGAUUC-3'; si-CHCHD3-1, 5'-UUCUUCAUCAGAAACUGAGGC-3'; si-CHCHD3-2, 5'-ACCAUAAGCACCAGAAUACCG-3'; and si-NC, 5'-UUCUCCGAACGUGUCACGU-3'. For overexpression experiments, plasmids encoding ASB1 (OE-ASB1) and CHCHD3 (OE-CHCHD3), and an empty vector were obtained from GenePharma (Suzhou, China) and transfected using Lipofectamine 2000. Cells were harvested 48 hours post-transfection for analysis. Reactive oxygen species (ROS) and ATP assays were measured using a ROS Advanced Fluorescence Assay Kit (Genmed Scientifics, Wilmington, DE, USA) and an ATP Measurement Kit (Beyotime, Nantong, China) [17], respectively.

Quantitative real-time PCR (qRT-PCR)

Total RNA was extracted from both prostate and adjacent non-tumor tissues, as well as from the PC3 and DU145 cell lines, using an RNeasy Plus Micro Kit (Qiagen, Düsseldorf, Germany). The study received prior approval from the relevant ethics committee. RNA was reverse transcribed to cDNA using a PrimeScript Reverse Transcription Kit (Vazyme, Nanjing, China). mRNA expression levels were

quantified using an ABI 7500 Real-Time PCR system (Applied Biosystems, Foster City, CA, USA) with SYBR Premix Ex Taq Polymerase (Takara, Dalian, China). 18S ribosomal RNA served as an internal control. The relative expression levels were calculated using the 2-ΔΔCt method, employing the following primers: ASB1 forward 5'-GAGTTGGGCTTCCCCTTACC-3' and reverse 5'-CACAATGGTCCTCATGGGCT-3'; CHCHD3 forward 5'-CGCTGTGCGGGAAAAGAATC-3' and reverse 5'-ATTTTCCGAAAGCCGGATGC-3'; 18S rRNA forward 5'-AAACGGCTACCACATCCAAG-3' and reverse 5'-CCTCCAATGGATCCTCGTTA-3'.

Tumor biological behavior assays

Cell viability was assessed using a CCK-8 kit (Beyotime) as previously described [18, 19]. Cells were seeded at a density of 5,000 cells per well in 96-well plates following various treatments. At 24-hour intervals, cells were incubated with 10% CCK-8 medium for 2 hours, and absorbance was measured at 450 nm using a microplate reader (Geneomaga).

For colony formation assays, approximately 500 cells were plated in six-well plates and cultured for 2 weeks. Cell colonies were fixed with 4% methanol for 15 minutes, stained with 0.1% crystal violet (Sigma-Aldrich) for 30 min and quantified using ImageJ software after being photographed.

Cell migration assays were conducted using transwell chambers. A 100 µl suspension of cells, post-treatment, was placed in the upper chamber of a transwell, with 600 µl of complete medium in the lower chamber. After 48 hours, cells remaining in the upper chamber were removed, while those that had migrated to the lower side were fixed with 4% paraformaldehyde, stained with 0.1% crystal violet (Beyotime) for 30 minutes, and counted under an inverted microscope across five randomly selected fields of view.

Lentiviral overexpression vector and Xenografts assay

The full-length of human ASB1 coding sequences was cloned into LV18/Puro lentiviral overexpression vector (GenePharma). For stable transfection, lentiviral LV18/Puro and packaging vectors were co-transfected into HEK-293T cells. The resultant viruses were collected from the supernatant and used to infect PC-3 cells, which were subsequently selected for puromycin resistance at 5 µg/mL puromycin for 2 weeks. In the mouse xenograft model, nude mice were injected subcutaneously with 5×10^6 PC-3 cells stably expressing either LV18/Puro-ASB1 or a control vector. Tumor growth was monitored every three days by measuring tumor volume and weight. Cellular proliferation within the tumors was evaluated through Ki67 immunofluorescence staining.

Immunofluorescence

Fresh 5-µm sections were prepared from paraffin-embedded samples of prostate cancer and control tissues. To minimize nonspecific antibody binding, sections were blocked with 5% (w/v) bovine serum albumin (Sunshine, Nanjing, China). Sections were then incubated overnight at 4°C with a primary antibody against Ki67 (Proteintech), followed by Alexa Fluor-conjugated secondary antibodies. Samples were counterstained with 4',6-diamidino-2-phenylindole and imaged using a confocal laser microscope (Zeiss LSM800, Carl Zeiss, Oberkochen, Germany) as previously described [20-22].

Western blotting

Western blotting was performed as previously described [23, 24]. In short, proteins were extracted from cell samples using RIPA buffer and separated by sodium dodecyl sulfate polyacrylamide gel electrophoresis (SDS-PAGE), then transferred onto polyvinylidene difluoride (PVDF) membranes (Millipore, Bedford, MA, USA). The membranes were blocked with 5% nonfat milk for 2 hours and incubated overnight at 4°C with the following primary antibodies: anti-Flag (1:1000; Sigma), anti-GFP (1:1000; Abcam), anti-tubulin (1:3000; Beyotime), anti-HA (1:1000; Santa Cruz), and anti-CHCHD3 (1:1000; Proteintech). After primary incubation, membranes were treated with HRP-conjugated secondary antibodies for 1 hour at room temperature and the target bands were visualized using an enhanced chemiluminescence substrate (Thermo Scientific, Waltham, USA).

Immunoprecipitation (IP) assays

For co-immunoprecipitation (Co-IP) assays [25], cell lysates were prepared by ysing cells in RIPA buffer (Beyotime, Nantong, China) on ice for 30 minutes. The lysates were then incubated with 20 μl of pre-washed Flag-Beads (Sigma) or GFP-Beads (Proteintech) for 8 hours at 4°C to immunoprecipitate Flag-tagged ASB1 or GFP-tagged CHCHD3, respectively. The supernatants were obtained for subsequent western blotting and liquid chromatography-tandem tandem MS (LC-MC/MS).

LC-MC/MS analysis

Protein samples were prepared by sequentially washing with deionized water, 50% acetonitrile, and 100% acetonitrile, followed by reduction and alkylation for 45 minutes at room temperature. After drying, the gels were rehydrated at 4°C for 30 minutes, and digested at 37°C for 12 hours. The resultant peptides were desalted using a StageTip and analyzed by an LTQ Orbitrap-Velos mass spectrometer. Tandem mass spectra were compared against the UniProt protein database to identify proteins and peptides with a 1% false discovery rate. Protein expression levels were quantified using the intensity-based absolute quantification (iBAQ) method via MaxQuant software [26]. All experiments were conducted in triplicate.

For analysis of protein interactions, protein sequences of ASB1 and CHCHD3 were retrieved in FASTA format from the NCBI. Three-dimensional structures were obtained from the Protein Data Bank or AlphaFold databases. The proteins to be analyzed were employed as RECeptor and LIGand models, respectively. The interactions between RECeptor and LIGand were examined using the HDOCK protein complex prediction tool [27]. The best docking model was selected to analyze the interactions between amino acids at the interaction interface. Visualizations and annotations of interacting residues were performed using PyMOL software (version: 2.1.0).

Protein half-life measurement

Following transfection with either pcDNA3.1 or pcDNA3.1-ASB1 vectors, prostate cancer cells were treated with CHX (100 μg/ml) at various time points to inhibit protein synthesis. The harvested proteins were subjected to protein blotting analysis at 0, 3, and 6 hours to assess levels of CHCHD3.

Statistical analysis

The data were analyzed using GraphPad Prism 9.0 (GraphPad, USA). Results represent the mean ± standard deviation from at least three independent experiments. Differences between two or more groups were assessed using Student's t-test or one-way analysis of variance (ANOVA), as appropriate. Statistical significance was established at a threshold of $P < 0.05$.

Results

ASB1 downregulation in prostate cancer

To investigate the potential role of ASB1 in prostate cancer progression, we analyzed expression levels in both tumor tissues and adjacent para-cancerous tissues using data from TCGA and GTEx. Our analysis revealed a significant downregulation of ASB1 expression in prostate cancer tissues compared to the para-cancerous tissues (**Figure 1A**). This trend became more pronounced when incorporating additional data from normal prostate tissues (GTEx) (**Figure 1B**). Notably, ASB1 exhibited decreased expression in 52 paired prostate cancer tissues from TCGA data (**Figure 1C**). To validate these findings, we conducted qRT-PCR to assess ASB1 expression in prostate cancer, confirming that confirmed the reduction in ASB1 expression in cancer tissues versus para-cancerous tissues (**Figure 1D**). In addition, receiver operating characteristic (ROC) curve analysis underscored the efficacy of ASB1 expression as a predictor, with an area under the curve (AUC) of 0.796 (**Figure 1E**), effectively distinguishing prostate cancer from normal tissue. Kaplan-Meier survival analysis revealed that low ASB1 expression correlates with poorer overall survival in prostate cancer patients (**Figure 1F**).

Employing the CIBERSORT algorithm, we quantified the proportion of immune cells in prostate cancer patients, categorizing them into high and low ASB1 expression groups. The low expression group exhibited a higher proportion of M2 macrophages compared with the high

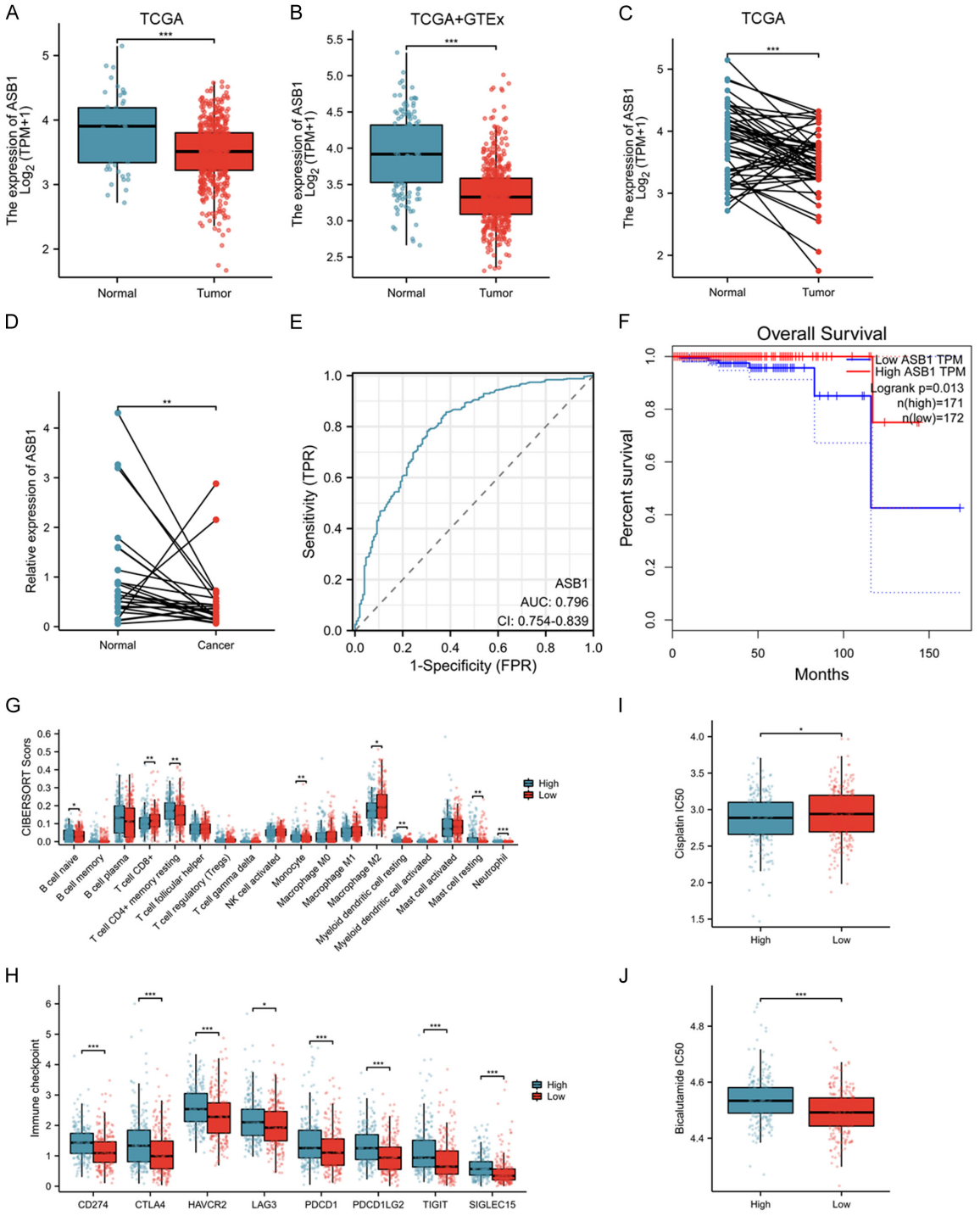

Figure 1. Low ASB1 expression is associated with prostate cancer progression. A. Comparative analysis showing downregulation of ASB1 in prostate cancer tissues (N = 501) versus para-cancerous tissues (N = 52) based on TCGA data. B. Analysis indicating downregulation of ASB1 in prostate cancer tissues (N = 496) compared to normal tissues (N = 152) using combined TCGA and GTEx data. C. ASB1 exhibited decreased expression in 52 paired prostate cancer tissues from TCGA. D. qRT-PCR assessment of ASB1 expression in cancerous and para-cancerous tissues in 26 prostate cancer patients. E. ROC curve analysis assessing the efficacy of ASB1 expression as a marker; the area under the curve (AUC) was 0.796, effectively distinguishing prostate cancer from normal tissue. F. Kaplan-Meier survival analysis revealing that low ASB1 expression was associated with poorer overall survival in prostate cancer patients. G. Use of the CIBERSORT algorithm to quantify immune cells proportions in prostate cancer patients with high and low ASB1 expression. H. Significant elevation in the expression of checkpoint molecules in the high ASB1

expression group compared to the low expression group. I, J. Exploration of ASB1 expression correlations with response to cisplatin (I) and AR-targeted drugs (J), analyzed by the pRRophetic algorithm. Significance levels indicated as *P < 0.05; **P < 0.01; ***P < 0.001.

expression group (**Figure 1G**). Comparative analysis of immune checkpoint molecule expression revealed significantly higher levels in the high ASB1 expression group (**Figure 1H**), suggesting potential enhanced immune escape and greater responsive to immunotherapy. To explore the correlation between ASB1 expression and chemotherapy response, we employed the pRRophetic algorithm. Our analysis indicated that patients in the high ASB1 expression group were sensitive to cisplatin but not to an androgen receptor (AR)-targeting drug, bicalutamide (**Figure 1I**, **1J**). These results underscore the potential of ASB1 to serve as a molecular marker for guiding chemotherapy and immunotherapy in prostate cancer patients.

Silencing ASB1 promotes prostate cancer cell proliferation in vitro

To gain a deeper understanding of ASB1's effects in prostate cancer, we conducted a series of experiments, including CCK-8 assays, transwell assays, and colony formation assays on prostate cancer cell lines DU145 and PC-3 transfected with si-ASB1. A notable reduction in ASB1 expression was observed (**Figure 2A**, **2B**). The results of the CCK-8 assay clearly showed a time-dependent increase in cell proliferation following ASB1 knockdown (**Figure 2C**, **2D**). Likewise, colony formation and transwell assays revealed substantial increases in both clonogenicity and cell migration in ASB1-siRNA-treated cells compared to controls (**Figure 2E-H**).

ASB1 overexpression inhibits prostate cancer cell biology in vitro and in vivo

To further substantiate the tumor-suppressor role of ASB1 in prostate cancer, DU145 and PC-3 cell lines were transfected with pcDNA3.1-ASB1-Flag plasmids (OE-ASB1) (**Figure 3A**). Subsequent CCK-8 assay revealed that ASB1 overexpression significantly reduced the growth of prostate cancer cells (**Figure 3B**, **3C**). Additionally, colony formation and cell migration were significantly reduced in ASB1-overexpressing cells compared to control cells (**Figure 3D-G**).

In vivo, xenograft assays in nude mice demonstrated that cells overexpressing ASB1 grew slower than those in the control group (**Figure 4A-D**). Immunofluorescence staining demonstrated a significant reduction in Ki67-positive cells, a proliferation marker, in the ASB1 overexpression group (**Figure 4E**, **4F**).

CHCHD3, a candidate binding protein for ASB1, affects prostate cancer cell biology

To investigate the underlying mechanism of ASB1, we performed IP-LC-MS/MS analyses using ASB1-overexpressing prostate cancer cells (**Figure 5A**) and identified 37 potential target proteins from three independent experiments. These included TCEB2, also known as ELOB, which ranked second according to iBAQ and is implicated in the formation of E3 ligase complexes with the ASB family [27] (**Figure 5B**, **5C**), suggesting that ASB1's role in protein ubiquitination degradation in prostate cancer. Furthermore, CHCHD3, among the top 10 candidate proteins by iBAQ (**Figure 5B**, **5C**), exhibits high expression in prostate cancer according to TCGA data (**Figure 5D**) and correlates with poor prognosis in prostate cancer patients (Figure S1A). CHCHD3, crucial for mitochondrial homeostasis, was further analyzed using gene set enrichment analysis (GSEA), comparing the ASB1 high and low expression groups in TCGA data (Figure S1B). The results revealed a significant enrichment of oxidative phosphorylation processes in the ASB1 low expression group, indicating that CHCHD3 as a potential target molecule through which ASB1 exerts its cancer inhibitory functions.

To examine the impact of CHCHD3 on the prostate cancer cell growth, we transfected prostate cancer cell lines DU145 and PC-3 with si-CHCHD3, resulting in a reduction in CHCHD3 expression compared to cells treated with si-NC (**Figures 5E** and S1C). Subsequent CCK-8 assay demonstrated that CHCHD3 inhibition in prostate cancer cells significantly suppressed cell viability in a time-dependent manner

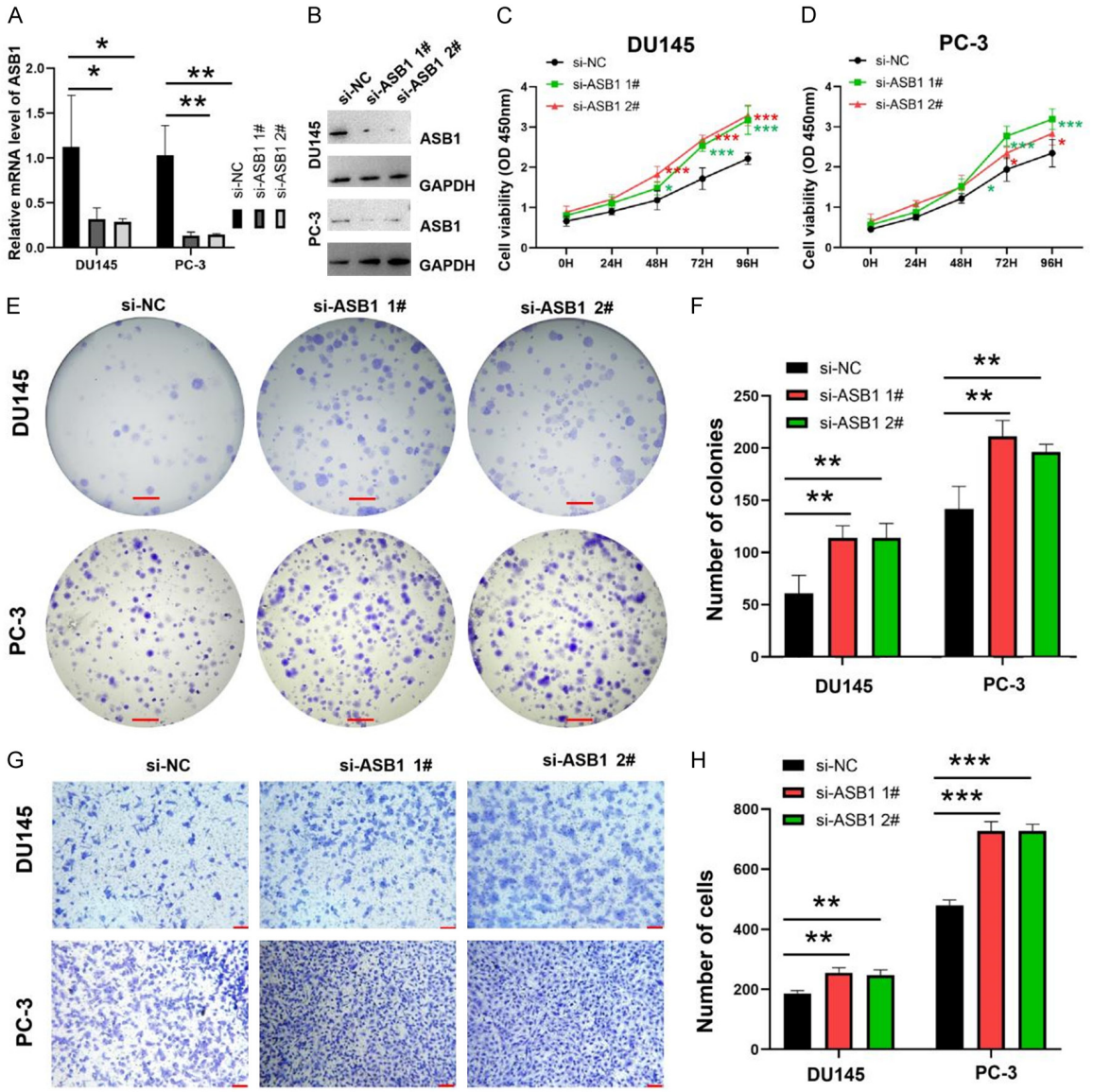

Figure 2. Silencing ASB1 promotes oncogenesis in prostate cancer cells. A. Quantitative real-time PCR analysis of ASB1 expression in DU145 and PC-3 cells transfected with si-NC and si-ASB1. B. Western blot analysis showing ASB1 protein levels in DU145 and PC-3 cells post-transfected with si-NC and si-ASB1. C, D. CCK-8 assay indicating a time-dependent increase in cell proliferation following ASB1 knockdown. E, F. Colony formation assays demonstrating increased clonogenicity in cells treated with ASB1-siRNA. Scale bar: 2 mm. G, H. Transwell assays revealing a substantial increase in numbers of migrating cells in the ASB1-siRNA-treated group compared to the control group. Scale bar: 100 μm. Significance levels indicated as *P < 0.05; **P < 0.01; ***P < 0.001.

(**Figure 5F**, **5G**). In addition, colony formation and migration were significantly reduced in CHCHD3-knockdown cells compared to controls (**Figure 5H-K**). Additionally, a significant increase in ROS and a decrease in ATP levels were also observed as a result of CHCHD3 knockdown (**Figure 5L**, **5M**), indicating its role in modulating tumor growth by regulating mitochondrial homeostasis.

ASB1 interacts with CHCHD3 and enhances its K48-linked ubiquitination

To substantiate the direct interaction between ASB1 and CHCHD3, we utilized bioinformatics tools such as HawkDock to predict the ASB1-CHCHD3 interaction and visualized it using PyMOL (**Figure 6A**). Immunostaining confirmed colocalization of ASB1 and CHCHD3 in DU145

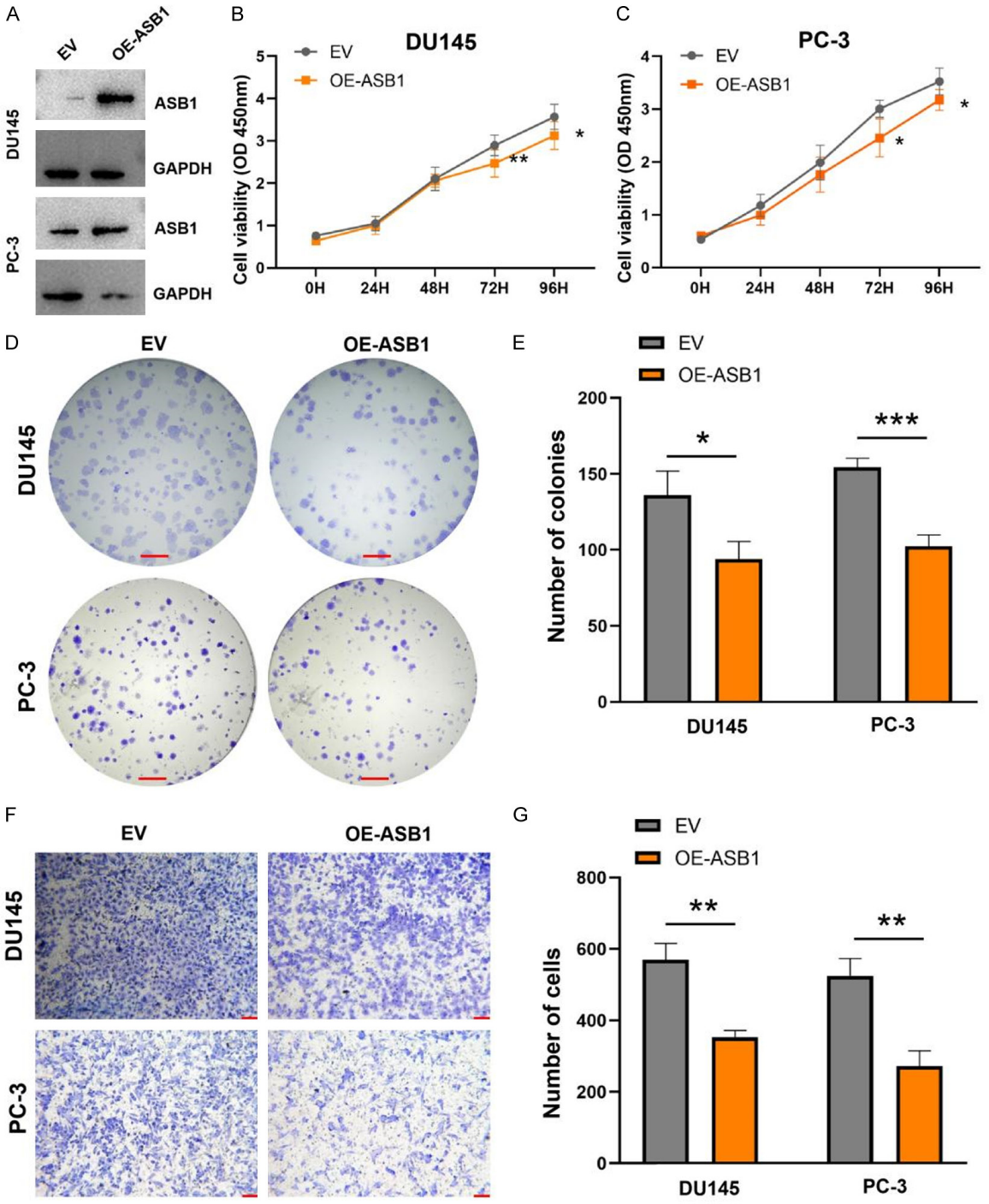

Figure 3. ASB1 overexpression inhibits prostate cancer cell biology. A. Western blot analysis showing ASB1 protein levels in DU145 and PC-3 cells transfected with EV and OE-ASB1 vectors. B, C. CCK-8 assays demonstrated that overexpression of ASB1 significantly reduces the growth of prostate cancer cells. D, E. Colony formation assays reveal a significantly reduced in clonogenicity in cells overexpressing ASB1. Scale bar: 2 mm. F, G. Transwell migration assays indicate a significant reduction in the number of migrating cells in the ASB1-overexpression group. Scale bar: 100 μm. Significance levels indicated as *P < 0.05; **P < 0.01; ***P < 0.001.

and PC-3 cells (Figure S2). Subsequent Co-IP experiments supported these bioinformatics models (**Figure 6B**). Western blotting and immunostaining demonstrated that ASB1 overexpression in DU145 and PC-3 cells reduced CHCHD3 protein levels, indicating that ASB1

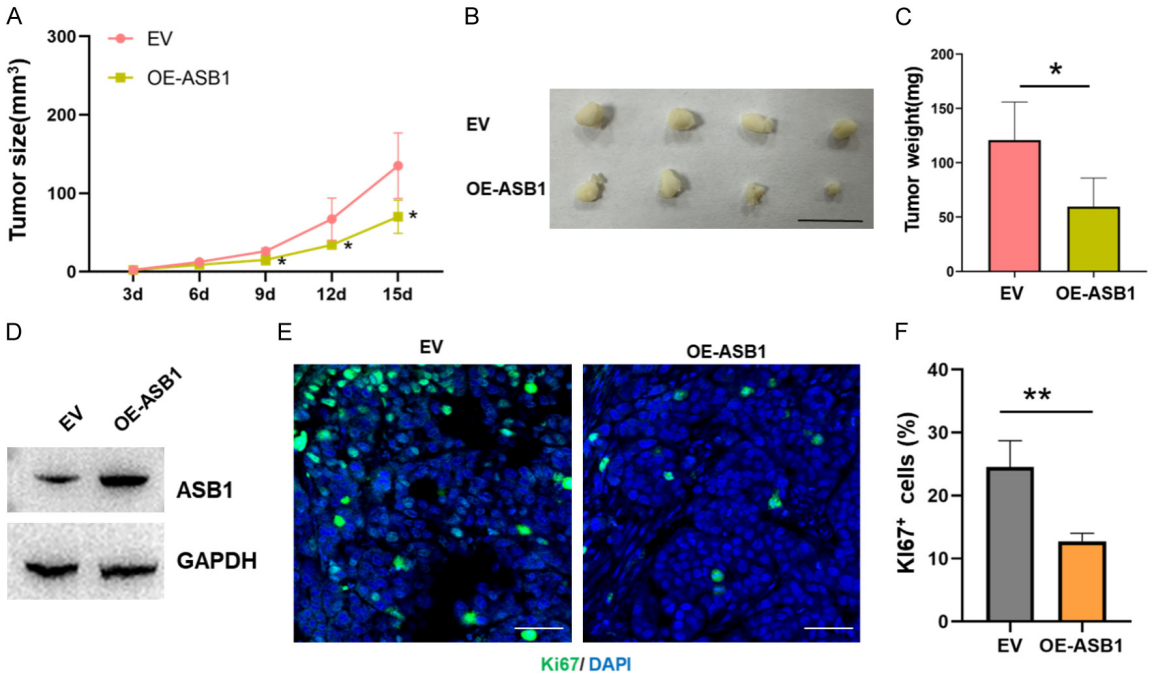

Figure 4. ASB1 overexpression reduces prostate cancer progression *in vivo*. A-C. Overexpressing ASB1 resulted in slower tumor growth compared to the control group. Scale bar: 1 cm. D. Western blot analysis confirming the overexpression efficiency of ASB1 in OE-ASB1 group. E, F. The number of Ki67-positive cells, indicative of proliferation, was significantly reduced in the ASB1 gene overexpression group. Scale bar: 50 μm. Significance levels indicated as *P < 0.05; **P < 0.01.

affects CHCHD3 protein stability (**Figures 6C** and S3). Treatment with CHX treatment significantly shortened the half-life of CHCHD3 after ASB1 overexpression (**Figure 6D**, **6E**). Moreover, ASB1 overexpression increased CHCHD3 polyubiquitination, particularly when MG132, a known proteasome inhibitor, was used (**Figure 6F**). In exploring K48 ubiquitination-mediated degradation, we transfected cells with Ub-K48O, Ub-K48R, and Ub-K0 mutants. Results demonstrated that both wild-type ubiquitin and K48O (Ub containing intact Lys48 residues only) could link to CHCHD3 via ASB1, while Ub-K0 failed to establish this linkage (**Figure 6G**). Notably, K48R (Ub mutated at the Lys48 residue only) mutants were not linked by ASB1 to CHCHD3 (**Figure 6G**), suggesting that ASB1 facilitates the CHCHD3 ubiquitination primarily through the K48 linkage.

N-acetylcysteine or CHCHD3 overexpression rescues the effect of ASB1 overexpression on prostate cancer cells in vitro

Given the inhibitory effects of ASB1 on prostate cancer cell viability and migration (**Figure 3**), alongside the promoting effects on ROS producing (Figure S4) and interaction with CHCHD3 (**Figure 6**), we investigated whether its cancer suppressor effects could be mediated via the CHCHD3 signaling pathway. Our investigation revealed that CHCHD3 overexpression, as well as administering N-acetylcysteine, a well-established antioxidant, effectively reversed the ASB1-induced alterations to proliferation (**Figure 7A**, **7B**), colony formation (**Figure 7C**, **7D**), and migration in DU145 and PC-3 cells (**Figure 7E**, **7F**).

Discussion

Prostate cancer ranks among the most prevalent malignancies affecting men, and its incidence continuing to rise annually [28]. Various treatment options are available including active surveillance and radical prostatectomy for localized cases [29]. For men with recurrent or metastatic prostate cancer, androgen deprivation therapy and chemotherapy are commonly employed. Despite advancements in these therapeutic approaches, prostate cancer remains largely incurable. The discovery of new molecules and mechanisms could enhance

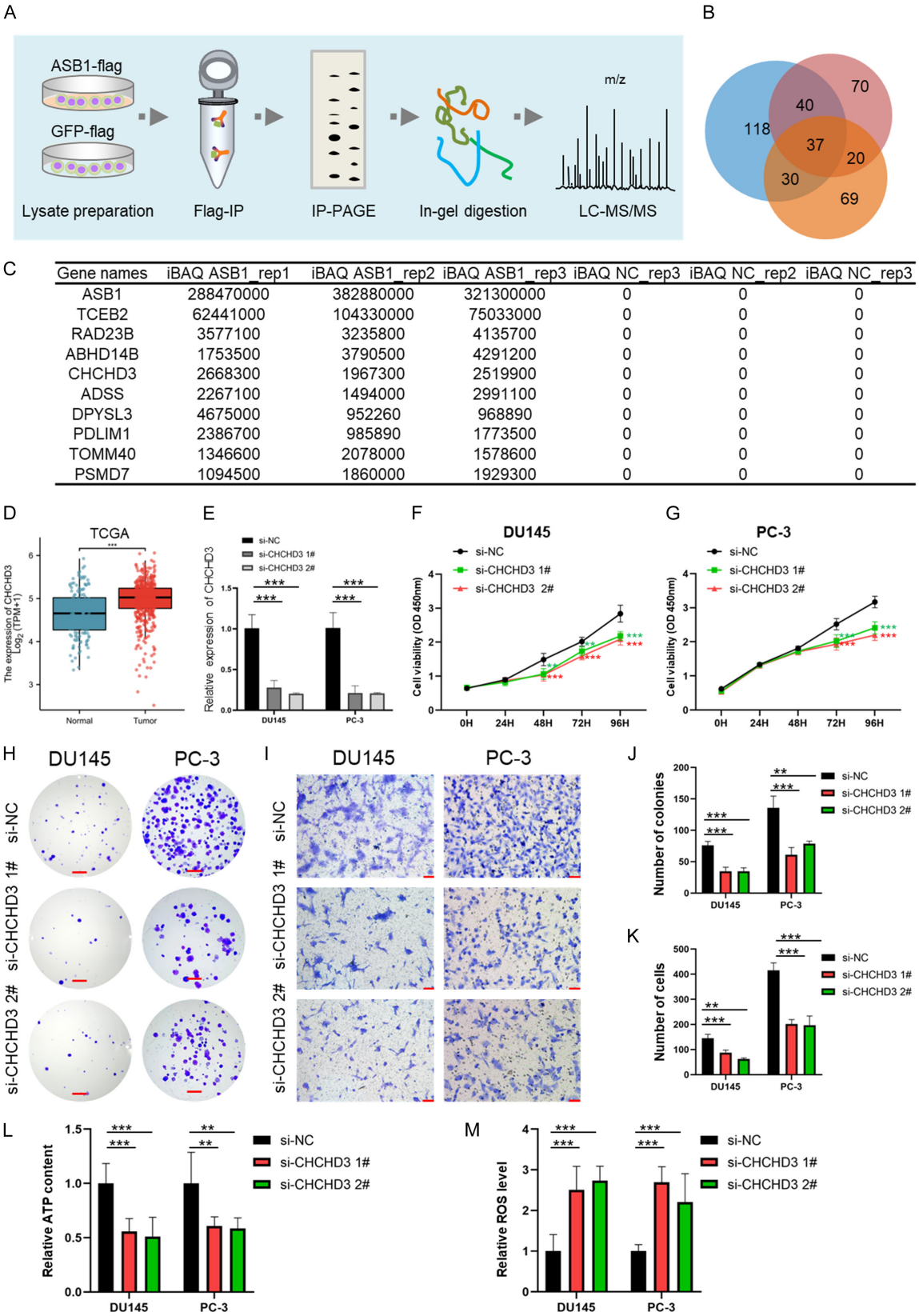

Gene names	iBAQ ASB1_rep1	iBAQ ASB1_rep2	iBAQ ASB1_rep3	iBAQ NC_rep3	iBAQ NC_rep2	iBAQ NC_rep3
ASB1	288470000	382880000	321300000	0	0	0
TCEB2	62441000	104330000	75033000	0	0	0
RAD23B	3577100	3235800	4135700	0	0	0
ABHD14B	1753500	3790500	4291200	0	0	0
CHCHD3	2668300	1967300	2519900	0	0	0
ADSS	2267100	1494000	2991100	0	0	0
DPYSL3	4675000	952260	968890	0	0	0
PDLIM1	2386700	985890	1773500	0	0	0
TOMM40	1346600	2078000	1578600	0	0	0
PSMD7	1094500	1860000	1929300	0	0	0

Figure 5. CHCHD3 as a candidate binding protein for ASB1 influences prostate cancer cell biology. (A) Flowchart illustrating the IP-MS analyses process: PC-3 cells were lysed post-transfection, followed by Flag-bead-based IP. The

IP products were then processed for SDS-PAGE, in-gel digestion, and LC-MC/MS analysis. (B) Venn diagrams showing the proteins identified by three independent IP-MS experiments. (C) List of the top ten potential target proteins of ASB1 according to iBAQ ranking. (D) Comparison of CHCHD3 expression in prostate cancer (N = 496) versus normal tissues (N = 152) using TCGA and GTEx data. (E) Knockdown of CHCHD3 expression in cells with si-CHCHD3. (F, G) CCK-8 assays demonstrating a time-dependent decrease in cell proliferation following CHCHD3 knockdown. (H-K) Significant reductions in the numbers of colony-forming and migrating cells in the CHCHD3-knockdown group compared to the control group. Scale bar: 2 mm for (H) and 100 μm for (I). (L) Observed decrease in ATP levels following CHCHD3 knockdown. (M) Notable increase in ROS levels after CHCHD3 knockdown. Significance levels indicated as **P < 0.01; ***P < 0.001.

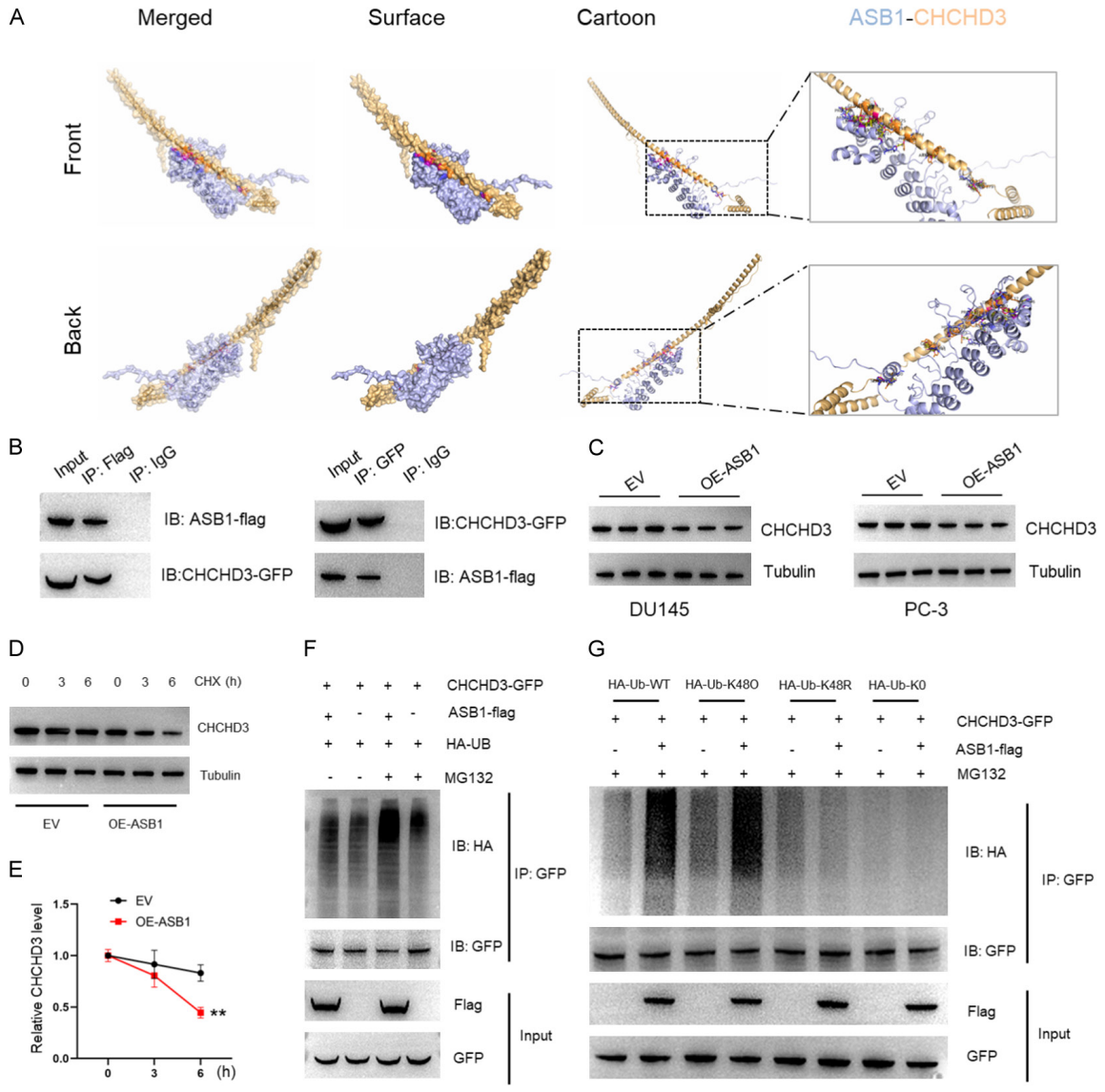

Figure 6. ASB1 interacts with CHCHD3 and affects its ubiquitination. A. Bioinformatics tools predicted ASB1-CCHD3 interaction. B. Co-IP experiments provided additional support for the bioinformatics predictions. C. Overexpression of ASB1 in DU145 and PC-3 cells resulted in decreased CHCHD3 protein levels. D, E. CHX treatment significantly shortened the half-life of CHCHD3 protein following ASB1 overexpression in PC-3 cells. F. ASB1 overexpression increased polyubiquitination of CHCHD3 in PC-3 cells, an effect that was amplified in the presence of the proteasome inhibitor MG132. G. ASB1 was primarily responsible for facilitating CHCHD3 ubiquitination through the K48 linkage. Significance levels indicated as **P < 0.01.

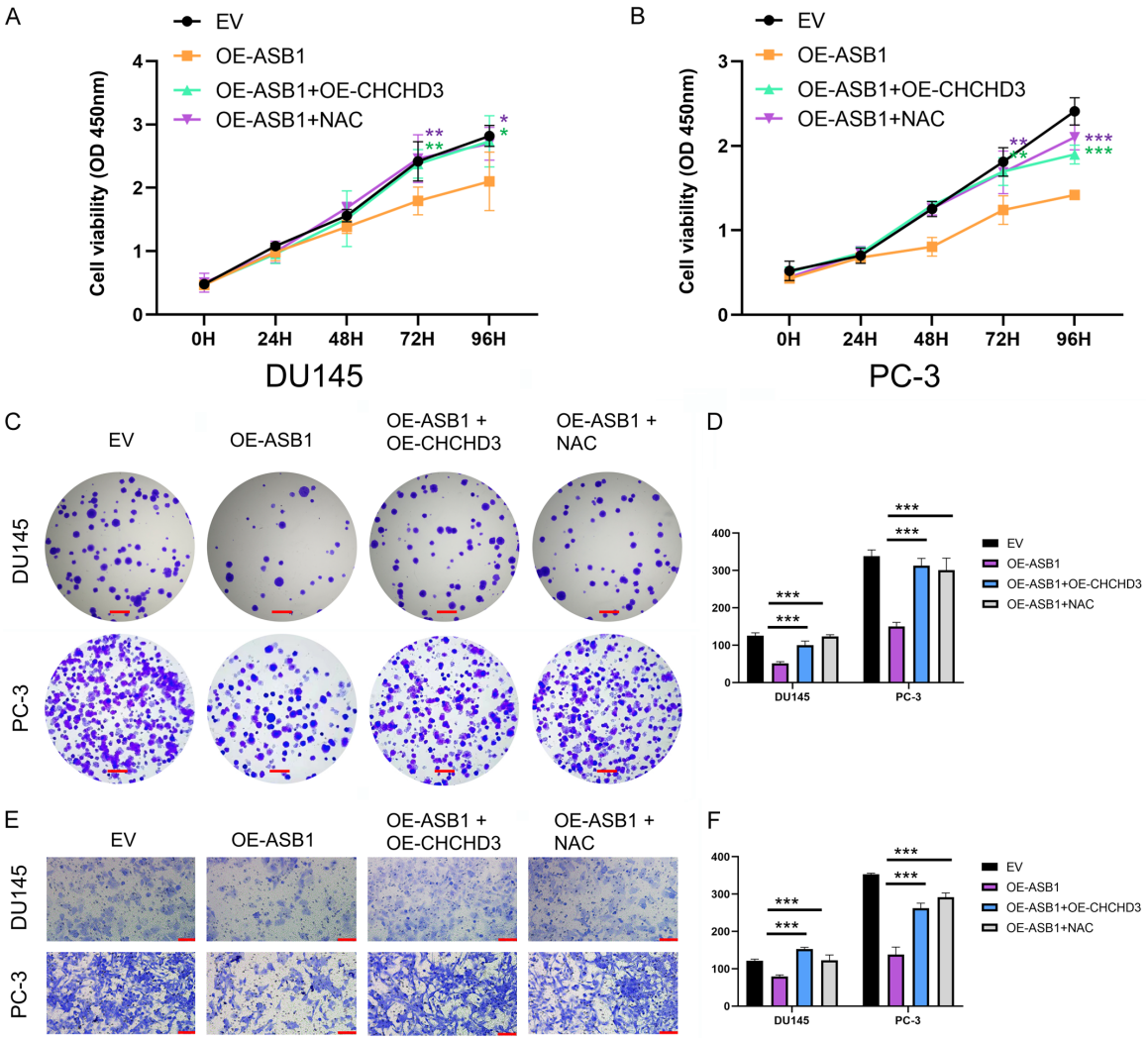

Figure 7. N-acetyl cysteine or CHCHD3 overexpression can reverse the impact of ASB1 overexpression on prostate cancer cells. A, B. CHCHD3 overexpression and application of N-acetylcysteine effectively attenuated the altered proliferation induced by ASB1 overexpression. C, D. Both CHCHD3 overexpression and application of N-acetylcysteine increased colony formation in ASB1-overexpressing cells. Scale bar: 2 mm. E, F. Transwell assays indicated that both CHCHD3-overexpressing and N-acetylcysteine-treated cells had increased migratory ability compared to ASB1-overexpressing cells. Scale bar: 100 μm. Significance levels indicated as *P < 0.05; **P < 0.01; ***P < 0.001.

early detection, enable disease stratification (distinguishing between indolent and aggressive cases), and improve predictions of treatment response, ultimately enhancing the prognosis for prostate cancer patients.

In the present study, we observed significant downregulation of ASB1 expression in prostate cancer tissues, correlating strongly with poor prognosis. This suggests that ASB1 may function as a novel tumor suppressor gene. Our experiments demonstrated that both knockdown and overexpression of ASB1 had profound effects on the biological behavior of prostate cancer cells, highlighting its potential role as a critical regulator in the progression of prostate cancer. Through Co-IP and MS analyses, we identified 37 potential binding proteins associated with ASB1. Among these, CHCHD3 emerged as a notable binding protein whose ubiquitination is regulated by ASB1, influencing its stability. This interaction has been implicated in the progression of prostate cancer, particularly through its involvement in oxidative stress pathways.

The ASB family consists of 18 members, predominantly ubiquitin E3 ligases, which play a

crucial role in the protein ubiquitination process and characterized by an ankyrin repeat and SOCS box domain [30, 31]. Previous studies have highlighted a strong association between ASB9 and ASB11 with tumor progression. However, the role of ASB1 in tumors, particularly in prostate cancer, has remained largely unknown. To investigate the potential role of ASB1 in prostate cancer, we conducted a comparative analysis of prostate cancer and normal prostate tissues using data from TCGA and GTEx. Our findings revealed significant downregulation of ASB1 expression in prostate cancer tissues, correlating strongly with poor prognosis. This initial observation prompted us to conduct qRT-PCR analysis on 26 cancerous and para-cancerous tissue samples, confirming substantial differences in ASB1 expression. These findings collectively suggest that ASB1 plays a part in the progression of prostate cancer. To substantiate our findings further, we performed both *in vitro* and *in vivo* experiments involving the knockdown and overexpression of ASB1. The knockdown of ASB1 led to increased proliferation and migration of prostate cancer cells, while its overexpression produced the opposite effect. To our knowledge, these findings provide the first comprehensive evidence that ASB1 may function as a key regulator in the progression of prostate cancer. In addition, the ASB1 low expression group in our study exhibited higher proportions of M2 macrophages [32], which are known to suppress inflammation, thereby promoting tumor proliferation and contributing to the immune escape mechanisms of tumor cells. This finding thus suggests a potential link between the poor prognosis associated with low ASB1 expression and the increased presence of M2 macrophages. Moreover, low ASB1 expression was associated with resistance to immune checkpoint inhibitors and cisplatin, yet showed sensitivity to the AR-targeting drug, bicalutamide. These results strongly suggest that ASB1 has the potential to serve as a valuable molecular marker guiding treatment strategies for prostate cancer patients.

ASB proteins function as E3 ubiquitin ligases, capable of recruiting target proteins for ubiquitination through anchor protein repeat sequences within their SOCS box structural domains [9, 33]. To investigate the potential binding of ASB1 to proteins for its cancer suppressor function, we conducted IP-LC-MS/MS analysis, which identified 37 potential target proteins. Notably, TCEB2 (also known as ELOB), ranked second according to iBAQ, is thought to form a SOCS box with the C-terminus of ASB proteins, thereby exerting E3 ubiquitin ligase activity. Among these, CHCHD3 emerged as a crucial binding protein. Located in the mitochondrial inner membrane, CHCHD3 is integral to maintaining mitochondrial homeostasis and influences tumor progression through its role in iron-mediated cell death and CD8+ T cell function [28, 34, 35]. High expression of CHCHD3, as observed in the TCGA data, was associated with a poor prognosis in prostate cancer. Interference with CHCHD3 expression in prostate cancer cell lines led to significant reductions in tumor progression and ATP production, accompanied by increased ROS levels.

Collectively, these observations suggest that CHCHD3 is pivotal in the pathogenesis of prostate cancer, potentially influenced by ASB1. Our subsequent Co-IP experiments, CHX treatment, and ubiquitination assays confirmed that ASB1 suppresses cancer by binding to CHCHD3 and promoting its ubiquitination. Rescue experiments further validated this interaction: CHCHD3 overexpression or use of antioxidant NAC reversed the effects of ASB1 overexpression on cell proliferation, migration, and colony formation. This provides additional evidence that ASB1 inhibits prostate cancer cell behaviors via its interaction with CHCHD3, affecting CHCHD3 ubiquitination and contributing to the elevation of ROS levels.

In summary, our study provides novel evidence that low ASB1 expression in prostate cancer correlates with an unfavorable prognosis and affects the effectiveness of immune checkpoint blockade, cisplatin, and AR-targeted drugs. Consequently, ASB1 shows promise as a valuable molecular marker for predicting treatment outcomes in prostate cancer. Furthermore, our mechanistic studies have revealed that ASB1 is a crucial suppressor in prostate cancer pathogenesis. ASB1 interacts with CHCHD3, regulating its stability through ubiquitination, and influences the progression of prostate cancer by affecting ROS levels.

Acknowledgements

This work was supported by the National Natural Science Foundation of China (82270-790 to RT) and the Suzhou Urological Disease Clinical Medical Center (Szlcyxzx202106 to CF).

Disclosure of conflict of interest

None.

Address correspondence to: Caibin Fan, Department of Urology, The Affiliated Suzhou Hospital of Nanjing Medical University, Suzhou 215002, Jiangsu, China. Tel: +86-18914029710; E-mail: fancaibin20@163.com; Ruoyun Tan, Department of Urology, The First Affiliated Hospital of Nanjing Medical University, Nanjing 210029, Jiangsu, China. Tel: +86-13952098899; E-mail: tanruoyun112@vip.sina.com

References

[1] Sung H, Ferlay J, Siegel RL, Laversanne M, Soerjomataram I, Jemal A and Bray F. Global cancer statistics 2020: GLOBOCAN estimates of incidence and mortality worldwide for 36 cancers in 185 countries. CA Cancer J Clin 2021; 71: 209-249.

[2] Sekhoacha M, Riet K, Motloung P, Gumenku L, Adegoke A and Mashele S. Prostate cancer review: genetics, diagnosis, treatment options, and alternative approaches. Molecules 2022; 27: 5730.

[3] Mohler JL, Antonarakis ES, Armstrong AJ, D'Amico AV, Davis BJ, Dorff T, Eastham JA, Enke CA, Farrington TA, Higano CS, Horwitz EM, Hurwitz M, Ippolito JE, Kane CJ, Kuettel MR, Lang JM, McKenney J, Netto G, Penson DF, Plimack ER, Pow-Sang JM, Pugh TJ, Richey S, Roach M, Rosenfeld S, Schaeffer E, Shabsigh A, Small EJ, Spratt DE, Srinivas S, Tward J, Shead DA and Freedman-Cass DA. Prostate cancer, version 2.2019, NCCN Clinical Practice Guidelines in Oncology. J Natl Compr Canc Netw 2019; 17: 479-505.

[4] Wang T, Jin C, Yang P, Chen Z, Ji J, Sun Q, Yang S, Feng Y, Tang J and Sun Y. UBE2J1 inhibits colorectal cancer progression by promoting ubiquitination and degradation of RPS3. Oncogene 2023; 42: 651-664.

[5] Vela-Rodríguez C and Lehtiö L. Activities and binding partners of E3 ubiquitin ligase DTX3L and its roles in cancer. Biochem Soc Trans 2022; 50: 1683-1692.

[6] Bian P, Dou Z, Jia Z, Li W and Pan D. Activated Wnt/β-Catenin signaling contributes to E3 ubiquitin ligase EDD-conferred docetaxel resistance in prostate cancer. Life Sci 2020; 254: 116816.

[7] Thomas E, Thankan RS, Purushottamachar P, Weber DJ and Njar VCO. Targeted degradation of androgen receptor by VNPP433-3β in castration-resistant prostate cancer cells implicates interaction with E3 ligase MDM2 resulting in ubiquitin-proteasomal degradation. Cancers (Basel) 2023; 15: 1198.

[8] Ma J, Zhou Y, Pan P, Yu H, Wang Z, Li LL, Wang B, Yan Y, Pan Y, Ye Q, Liu T, Feng X, Xu S, Wang K, Wang X, Jian Y, Ma B, Fan Y, Gao Y, Huang H and Li L. TRABID overexpression enables synthetic lethality to PARP inhibitor via prolonging 53BP1 retention at double-strand breaks. Nat Commun 2023; 14: 1810.

[9] Liu P, Verhaar AP and Peppelenbosch MP. Signaling size: ankyrin and SOCS Box-containing ASB E3 ligases in action. Trends Biochem Sci 2019; 44: 64-74.

[10] Liu Y, Li X, He Y, Wang H, Gao M, Han L, Qiu D, Ling L, Liu H and Gu L. ASB7 is a novel regulator of cytoskeletal organization during oocyte maturation. Front Cell Dev Biol 2020; 8: 595917.

[11] Kile BT, Metcalf D, Mifsud S, DiRago L, Nicola NA, Hilton DJ and Alexander WS. Functional analysis of Asb-1 using genetic modification in mice. Mol Cell Biol 2001; 21: 6189-6197.

[12] Ortega A, Tarazón E, Gil-Cayuela C, Martínez-Dolz L, Lago F, González-Juanatey JR, Sandoval J, Portolés M, Roselló-Lletí E and Rivera M. ASB1 differential methylation in ischaemic cardiomyopathy: relationship with left ventricular performance in end-stage heart failure patients. ESC Heart Fail 2018; 5: 732-737.

[13] Emeny RT, Baumert J, Zannas AS, Kunze S, Wahl S, Iurato S, Arloth J, Erhardt A, Balsevich G, Schmidt MV, Weber P, Kretschmer A, Pfeiffer L, Kruse J, Strauch K, Roden M, Herder C, Koenig W, Gieger C, Waldenberger M, Peters A, Binder EB and Ladwig KH. Anxiety associated increased CpG methylation in the promoter of Asb1: a translational approach evidenced by epidemiological and clinical studies and a murine model. Neuropsychopharmacology 2018; 43: 342-353.

[14] Yang XY, Ren CP, Wang L, Li H, Jiang CJ, Zhang HB, Zhao M and Yao KT. Identification of differentially expressed genes in metastatic and non-metastatic nasopharyngeal carcinoma cells by suppression subtractive hybridization. Cell Oncol 2005; 27: 215-223.

[15] Zhou J, Li J, Qian C, Qiu F, Shen Q, Tong R, Yang Q, Xu J, Zheng B, Lv J and Hou J. LINC00624/TEX10/NF-κB axis promotes proliferation and migration of human prostate cancer cells. Biochem Biophys Res Commun 2022; 601: 1-8.

[16] Xu W, Wang J, Xu J, Li S, Zhang R, Shen C, Xie M, Zheng B and Gu M. Long non-coding RNA

DEPDC1-AS1 promotes proliferation and migration of human gastric cancer cells HGC-27 via the human antigen R-F11R pathway. J Int Med Res 2022; 50: 3000605221093135.
[17] Shen C, Li M, Zhang P, Guo Y, Zhang H, Zheng B, Teng H, Zhou T, Guo X and Huo R. A comparative proteome profile of female mouse gonads suggests a tight link between the electron transport chain and meiosis initiation. Mol Cell Proteomics 2018; 17: 31-42.
[18] Wang Q, Wu Y, Lin M, Wang G, Liu J, Xie M, Zheng B, Shen C and Shen J. BMI1 promotes osteosarcoma proliferation and metastasis by repressing the transcription of SIK1. Cancer Cell Int 2022; 22: 136.
[19] Zhang K, Xu J, Ding Y, Shen C, Lin M, Dai X, Zhou H, Huang X, Xue B and Zheng B. BMI1 promotes spermatogonia proliferation through epigenetic repression of Ptprm. Biochem Biophys Res Commun 2021; 583: 169-177.
[20] Zhou H, Shen C, Guo Y, Huang X, Zheng B and Wu Y. The plasminogen receptor directs maintenance of spermatogonial stem cells by targeting BMI1. Mol Biol Rep 2022; 49: 4469-4478.
[21] Xue J, Wu T, Huang C, Shu M, Shen C, Zheng B and Lv J. Identification of proline-rich protein 11 as a major regulator in mouse spermatogonia maintenance via an increase in BMI1 protein stability. Mol Biol Rep 2022; 49: 9555-9564.
[22] Wu Y, Shen C, Wu T, Huang X, Li H and Zheng B. Syntaxin binding protein 2 in sertoli cells regulates spermatogonial stem cell maintenance through directly interacting with connexin 43 in the testes of neonatal mice. Mol Biol Rep 2022; 49: 7557-7566.
[23] Shen C, Yu J, Zhang X, Liu CC, Guo YS, Zhu JW, Zhang K, Yu Y, Gao TT, Yang SM, Li H, Zheng B and Huang XY. Strawberry Notch 1 (SBNO1) promotes proliferation of spermatogonial stem cells via the noncanonical Wnt pathway in mice. Asian J Androl 2019; 21: 345-350.
[24] Wu Y, Wang T, Zhao Z, Liu S, Shen C, Li H, Liu M, Zheng B, Yu J and Huang X. Retinoic Acid induced protein 14 (Rai14) is dispensable for mouse spermatogenesis. PeerJ 2021; 9: e10847.
[25] Yu X, Xu B, Gao T, Fu X, Jiang B, Zhou N, Gao W, Wu T, Shen C, Huang X, Wu Y and Zheng B. E3 ubiquitin ligase RNF187 promotes growth of spermatogonia via lysine 48-linked polyubiquitination-mediated degradation of KRT36/KRT84. FASEB J 2023; 37: e23217.
[26] Liu Y, Yu X, Huang A, Zhang X, Wang Y, Geng W, Xu R, Li S, He H, Zheng B, Chen G and Xu Y. INTS7-ABCD3 interaction stimulates the proliferation and osteoblastic differentiation of mouse bone marrow mesenchymal stem cells by suppressing oxidative stress. Front Physiol 2021; 12: 758607.
[27] Yan Y, Tao H, He J and Huang SY. The HDOCK server for integrated protein-protein docking. Nat Protoc 2020; 15: 1829-1852.
[28] Darshi M, Mendiola VL, Mackey MR, Murphy AN, Koller A, Perkins GA, Ellisman MH and Taylor SS. ChChd3, an inner mitochondrial membrane protein, is essential for maintaining crista integrity and mitochondrial function. J Biol Chem 2011; 286: 2918-2932.
[29] Schaeffer EM, Srinivas S, Adra N, An Y, Barocas D, Bitting R, Bryce A, Chapin B, Cheng HH, D'Amico AV, Desai N, Dorff T, Eastham JA, Farrington TA, Gao X, Gupta S, Guzzo T, Ippolito JE, Kuettel MR, Lang JM, Lotan T, McKay RR, Morgan T, Netto G, Pow-Sang JM, Reiter R, Roach M, Robin T, Rosenfeld S, Shabsigh A, Spratt D, Teply BA, Tward J, Valicenti R, Wong JK, Berardi RA, Shead DA and Freedman-Cass DA. NCCN Guidelines® insights: prostate cancer, version 1.2023. J Natl Compr Canc Netw 2022; 20: 1288-1298.
[30] Luo L, Zhang W and Li Z. LncRNA HAGLR may aggravate melanoma malignancy via miR-4644/ASB11 pathway. Mol Biotechnol 2023; 65: 1619-1631.
[31] Tokuoka M, Miyoshi N, Hitora T, Mimori K, Tanaka F, Shibata K, Ishii H, Sekimoto M, Doki Y and Mori M. Clinical significance of ASB9 in human colorectal cancer. Int J Oncol 2010; 37: 1105-1111.
[32] Wu H, Feng J, Zhong W, Zouxu X, Xiong Z, Huang W, Zhang C, Wang X and Yi J. Model for predicting immunotherapy based on M2 macrophage infiltration in TNBC. Front Immunol 2023; 14: 1151800.
[33] Linossi EM and Nicholson SE. The SOCS box-adapting proteins for ubiquitination and proteasomal degradation. IUBMB Life 2012; 64: 316-323.
[34] Xue X, Ma L, Zhang X, Xu X, Guo S, Wang Y, Qiu S, Cui J, Guo W, Yu Y, Sun F, Shi Y and Wang J. Tumour cells are sensitised to ferroptosis via RB1CC1-mediated transcriptional reprogramming. Clin Transl Med 2022; 12: e747.
[35] Ogando J, Sáez ME, Santos J, Nuevo-Tapioles C, Gut M, Esteve-Codina A, Heath S, González-Pérez A, Cuezva JM, Lacalle RA and Mañes S. PD-1 signaling affects cristae morphology and leads to mitochondrial dysfunction in human CD8(+) T lymphocytes. J Immunother Cancer 2019; 7: 151.

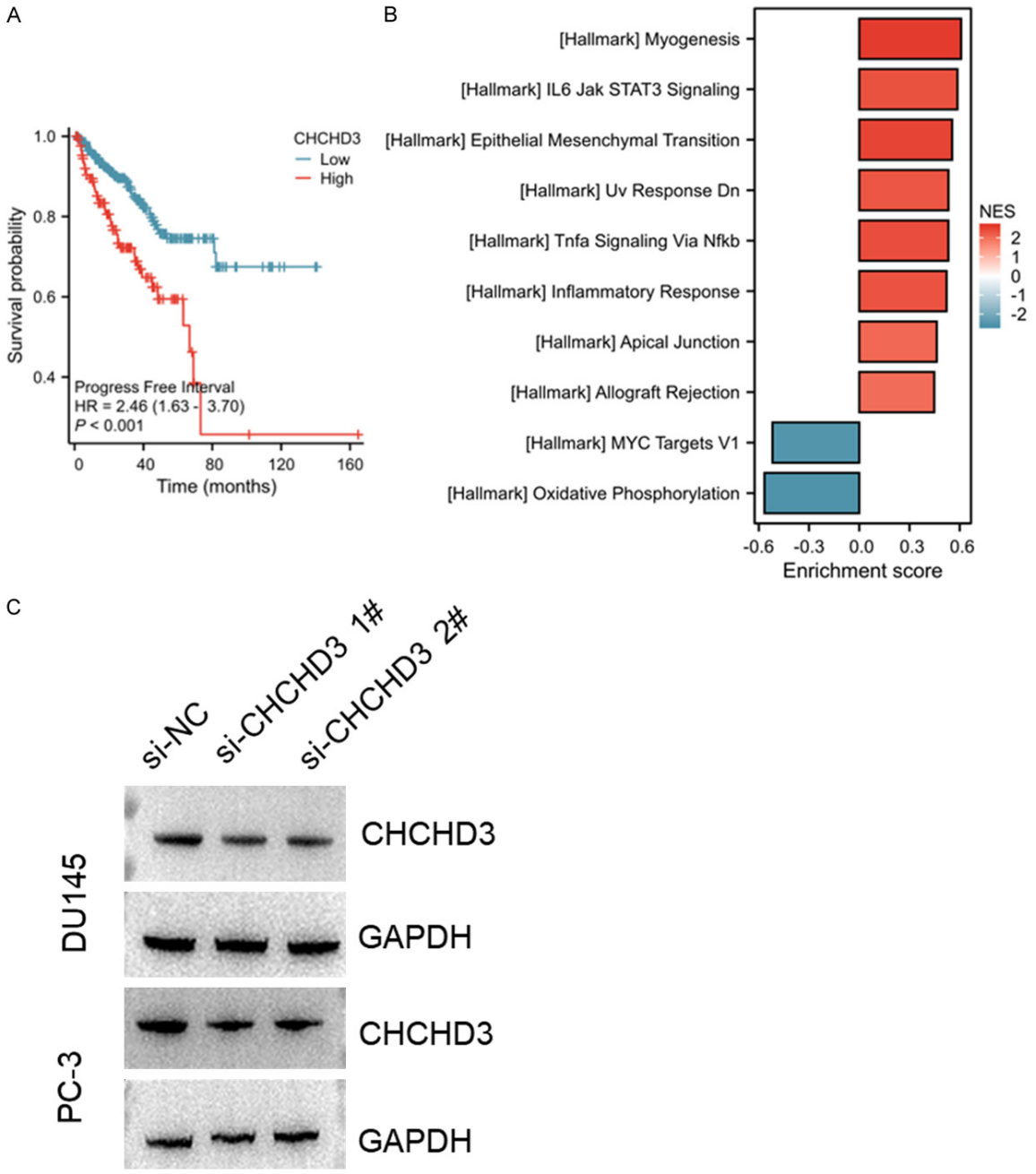

Figure S1. CHCHD3 is a candidate binding protein for ASB1. A. High CHCHD3 expression correlated with poor prognosis in prostate cancer. B. Gene set enrichment analysis reveals significant enrichment of oxidative phosphorylation processes in the ASB1 low expression group. C. Western blot analysis confirming the knockdown efficiency of CHCHD3 in DU145 and PC-3 cells transfected with si-NC and si-CHCHD3.

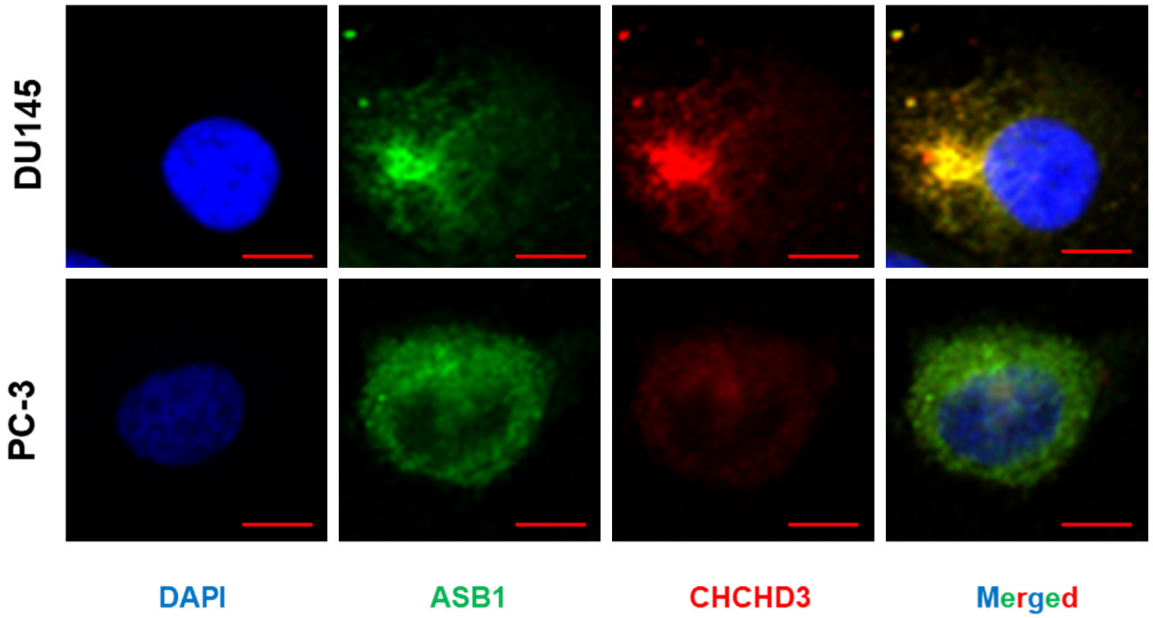

Figure S2. Colocalization of ASB1 with CHCHD3. Co-immunostaining demonstrates colocalization of ASB1 and CHCHD3 in DU145 and PC-3 cells. Scale bar: 10 μm.

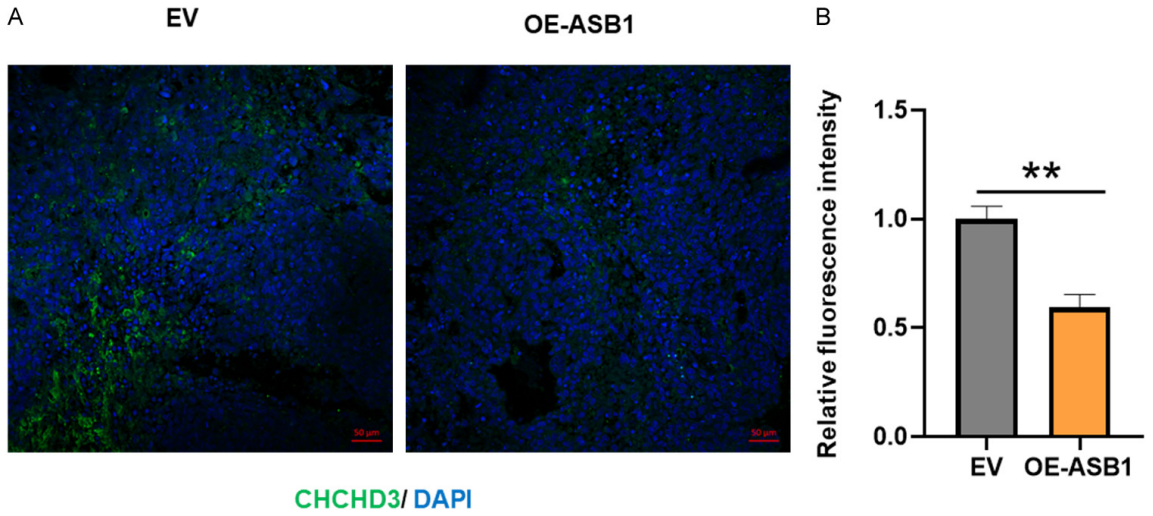

Figure S3. Reduction of CHCHD3 expression due to ASB1 overexpression. (A) Immunostaining of CHCHD3 in tumor tissues treated with empty vector (EV) and overexpression vector for ASB1 (OE-ASB1). Scale bar: 50 μm. (B) Quantification of immunostaining intensity from (A).

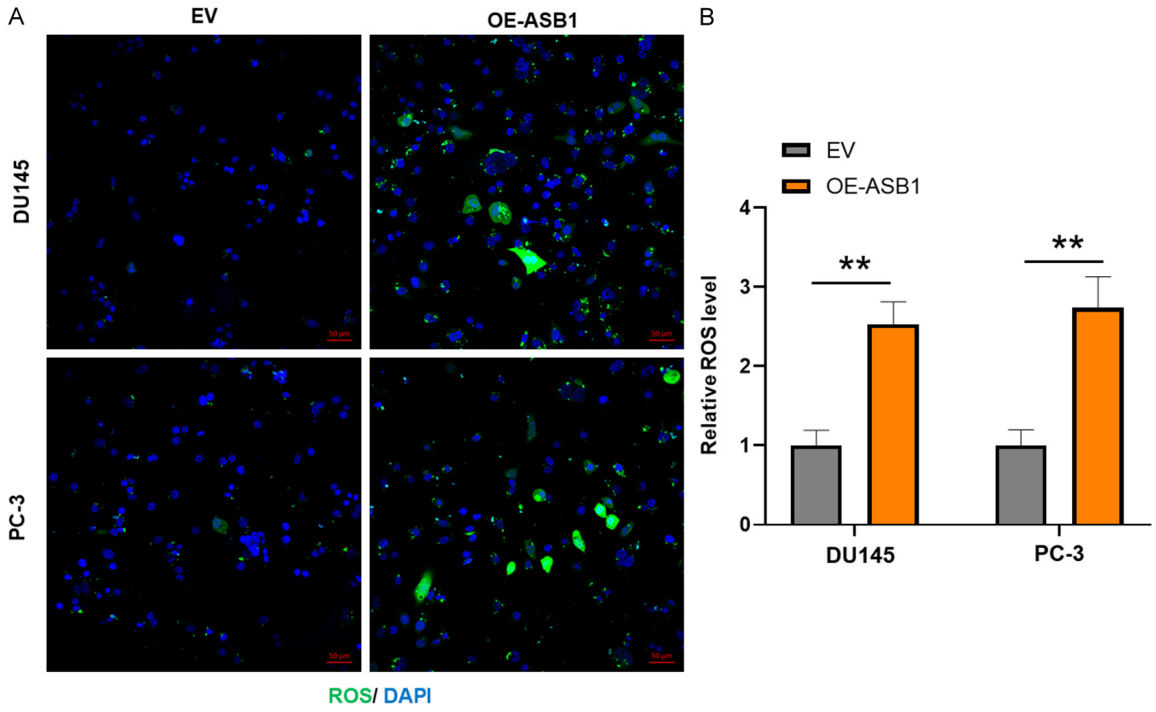

Figure S4. ASB1 overexpression induces ROS production. (A) ROS assays in DU145 and PC-3 cells transfected with empty vector (EV) and ASB1 overexpression vector (OE-ASB1). Scale bar: 50 μm. (B) Quantification of ROS production from (A).